Computer Physics Communications 261 (2021) 107825

Contents lists available at ScienceDirect

Computer Physics Communications

journal homepage: www.elsevier.com/locate/cpc

A variant of stabilized-scalar auxiliary variable (S-SAV) approach for a modified phase-field surfactant model☆

Junxiang Yang, Junseok Kim *

Department of Mathematics, Korea University, Seoul, 02841, Republic of Korea

ARTICLE INFO

Article history:
Received 28 July 2020
Received in revised form 8 December 2020
Accepted 27 December 2020
Available online 8 January 2021

Keywords:
New S-SAV approach
Modified phase-field surfactant
Second-order accuracy
Energy stability

ABSTRACT

In this article, we develop a new linear, decoupled, second-order accurate, and energy stable numerical method for a modified phase-field surfactant model (Xu et al., 2020). The proposed scheme is a simple and efficient variant of stabilized-scalar auxiliary variable (S-SAV) method. The proposed scheme not only retains all advantages of S-SAV method but also simplifies the solution algorithm. The phase-field, surfactant, and auxiliary variables are totally decoupled in time, thus we can solve the whole system in a step-by-step manner. The phase-field function ϕ and surfactant ψ can be separately updated by solving two linear semi-implicit systems with constant coefficients and then the auxiliary variable is directly updated in an explicit way. We analytically prove the energy stability and the unique solvability of the proposed method. The numerical experiments show the desired temporal accuracy and energy stability. We numerically investigate the proper stabilization coefficients for the present scheme with specific parameters. Furthermore, various two- and three-dimensional benchmark tests are performed to study the dynamics of surfactant-laden phase separation.

1. Introduction

The surfactant is an amphiphilic organic compound, which contains a hydrophilic head and a hydrophobic tail. Due to its special structure, the surfactant has various applications in industrial fields, such as food processing [1], liquid emulsion [2], and oil recovery [3,4], etc. To numerically study the dynamics of surfactant, some successful works had been performed based on volume-of fluid method [5], level-set method [6,7], immersed boundary method [8], lattice Boltzmann method [9], and phase-field method [3,10,11] in the past twenty years. In a pioneering work, Laradji et al. [12] studied the effect of surfactant on phase separation. Recently, Engblom et al. [13] used the phase-field method to simulate the dynamics of surfactant in two-phase flow systems. In phase-field model, many governing equations can be derived from a free energy functional. In general, the free energy functional has a basic physical property, i.e., energy dissipation law. To preserve this important property in computational simulation, researchers recently developed energy dissipation preserving numerical methods for the phase-field surfactant models.

Based on the convex splitting approach, Gu et al. [14] developed an energy stable finite difference method for the binary phase-field surfactant system. Recently, the invariant energy quadratization (IEQ) approach and the scalar auxiliary variable (SAV) approach become popular for phase-field models. Based on the IEQ approach, Yang [15] developed linear and energy stable method for a phase-field surfactant model. However, the analytical energy estimation only holds for temporally first-order scheme. Later, Yang and Ju [16] constructed second-order accurate and energy stable method for a modified model by using the IEQ approach. Zhu et al. [17] proposed an efficient and energy stable scheme for a phase-field surfactant with Flory–Huggins potential by using the classical SAV approach, however the strict energy estimation is valid only for first-order accurate scheme. Zhu et al. [18] later extended their method to the phase-field surfactant model with incompressible fluid flows. Based on the SAV approach, Sun et al. [19] numerically investigated the dynamics of phase-field surfactant system on various curved surfaces.

In this study, we consider a recently developed phase-field surfactant model [20]. Let ϕ be the phase-field variable which is close to 1 in one phase and -1 in the other phase. The total energy functional on Ω can be expressed as

$$\mathcal{E}(\phi, \psi) = \mathcal{E}_1(\phi) + \mathcal{E}_2(\psi) + \mathcal{E}_3(\phi, \psi), \tag{1}$$

where

$$\mathcal{E}_1(\phi) = \int_\Omega \left(\frac{\gamma_1}{2} |\nabla \phi|^2 + F(\phi) \right) d\mathbf{x}, \tag{2}$$

☆ The review of this paper was arranged by Prof. D.P. Landau.

* Corresponding author.
E-mail address: cfdkim@korea.ac.kr (J. Kim).
URL: http://math.korea.ac.kr/~cfdkim (J. Kim).

https://doi.org/10.1016/j.cpc.2021.107825
0010-4655/

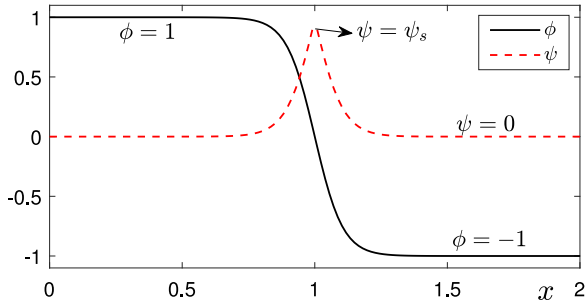

Fig. 1. Schematic illustration of surfactant distribution across two-phase fluid interface.

$$\mathcal{E}_2(\psi) = \int_\Omega \left(\frac{\gamma_2}{2}|\nabla\psi|^2 + G(\psi)\right) d\mathbf{x}, \tag{3}$$

$$\mathcal{E}_3(\phi, \psi) = \int_\Omega \left(-\frac{\theta}{2}\psi|\nabla\phi|^2 + \frac{\xi}{4}|\nabla\phi|^4\right) d\mathbf{x}, \tag{4}$$

$$F(\phi) = \frac{1}{4\epsilon^2}\left(\phi^2 - 1\right)^2, \tag{5}$$

$$G(\psi) = \frac{1}{4\eta^2}\psi^2(\psi - \psi_s)^2. \tag{6}$$

The parameters γ_1, γ_2, θ, ξ, ϵ, and η are all positive. In $\mathcal{E}_1(\phi)$, the fourth-order polynomial potential $F(\phi)$ describes the phase separation and the gradient term $|\nabla\phi|^2$ leads to the mixing. In $\mathcal{E}_2(\psi)$, $G(\psi)$ is another fourth-order polynomial potential which makes the surfactant concentration equal to zero in the bulk phases ($\phi = \pm 1$) and reach its maximum ψ_s at the interface $\phi = 0$. Here, ψ_s is considered as the density of condensed hydrocarbon chains of surfactant [20]. The one-dimensional illustration of surfactant-laden two-phase system at equilibrium state is shown in Fig. 1. In $\mathcal{E}_3(\phi, \psi)$, the coupling term $-\frac{\theta}{2}\psi|\nabla\phi|^2$ is important in the interaction of fluid mixture and surfactant. It describes the concentration of surfactant accumulates on the interface. However, this part is not strictly bounded from below because ψ is positive. Hence, Xu et al. [20] added the term $\frac{\xi}{4}|\nabla\phi|^4$ to fix this problem. Similar idea can also be found in [21]. Note for any $\xi > 0$, we have

$$-\frac{\theta}{2}\psi|\nabla\phi|^2 + \frac{\xi}{4}|\nabla\phi|^4 = \frac{\xi}{4}(|\nabla\phi|^2 - \frac{\theta}{\xi}\psi)^2 - \frac{\theta^2}{4\xi}\psi^2. \tag{7}$$

It is obvious that the last negative term can be bounded by the fourth-order polynomial term in $\mathcal{E}_2(\psi)$.

By taking the variational derivatives of Eq. (1) with respect to ϕ and ψ, we have

$$\phi_t = M_\phi \Delta\mu_\phi, \tag{8}$$

$$\mu_\phi = -\gamma_1\Delta\phi - \xi\nabla\cdot(|\nabla\phi|^2\nabla\phi) + F'(\phi) + \theta\nabla\cdot(\psi\nabla\phi), \tag{9}$$

$$\psi_t = M_\psi \Delta\mu_\psi, \tag{10}$$

$$\mu_\psi = -\gamma_2\Delta\psi + G'(\psi) - \frac{\theta}{2}|\nabla\phi|^2, \tag{11}$$

where the subscript t indicates the time derivative, $F'(\phi) = \frac{1}{\epsilon^2}(\phi^3 - \phi)$, $G'(\psi) = \frac{1}{\eta^2}\psi(\psi - \psi_s)(\psi - \frac{\psi_s}{2})$, M_ϕ and M_ψ are positive and constant mobilities. On all boundaries of domain Ω, we can use the periodic boundary condition or zero-Neumann boundary condition, i.e., $\partial_{\mathbf{n}}\phi|_{\partial\Omega} = \partial_{\mathbf{n}}\psi|_{\partial\Omega} = \nabla\mu_\phi\cdot\mathbf{n}|_{\partial\Omega} = \nabla\mu_\psi\cdot\mathbf{n}|_{\partial\Omega} = 0$, where $\mathbf{n}$ represents the unit normal vector to the boundary $\partial\Omega$. We can prove that the system (8)–(11) combining with the above boundary conditions satisfies the mass conservation, i.e.,

$$\frac{d}{dt}\int_\Omega \phi d\mathbf{x} = \frac{d}{dt}\int_\Omega \psi d\mathbf{x} = 0. \tag{12}$$

Then, we define the operations $(\cdot,\cdot)$ and $\|\cdot\|$ be the L^2-inner product and its norm. By taking the L^2-inner product of Eq. (8) with μ_ϕ, Eq. (9) with $-\phi_t$, of Eq. (10) with μ_ψ, of Eq. (11) with $-\psi_t$, and combining them together, we can show the following energy law

$$\frac{d}{dt}\mathcal{E}(\phi, \psi) = -M_\phi\|\nabla\mu_\phi\|^2 - M_\psi\|\nabla\mu_\psi\|^2 \le 0, \tag{13}$$

where the integration by parts is used. This indicates the system satisfies the energy dissipation.

To solve this phase-field surfactant model (8) and (9), Xu et al. [20] presented an efficient, second-order accurate, and linear numerical scheme by using the stabilized-scalar auxiliary variable (S-SAV) approach. In their work, the phase-field functions and auxiliary variables are still coupled with each other. In this study, we develop an alternative numerical scheme based on a recently developed step-by-step solving SAV approach [22]. In the proposed method, the phase-field function, surfactant, and auxiliary variable are totally decoupled in time. We only need to solve two semi-implicit systems with constant coefficients and then directly update auxiliary variable by an explicit way. For the SAV type method, the basic idea is to change the original equations into an equivalent form by using a time-dependent auxiliary variable. In actual computation, all nonlinear terms are treated explicitly for the purpose of efficiency. However, explicit nonlinear terms will affect the accuracy if time step is large enough or the nonlinear effect is dominant. To maintain the desired accuracy at some larger time steps, the stabilization technique [20,23,24] is adopted, where two extra linear stabilization terms are added to suppress the nonlinear effects and enhance the stability. We numerically validate this in Section 4.1. The errors caused by the extra linear stabilization terms are of the order $C_\phi(\Delta t)^p\phi(\cdot)$ and $C_\psi(\Delta t)^p\psi(\cdot)$ [20], where C_ϕ and C_ψ are constants, Δt is the time step, $p = 1$ or 2 with respect to the first- or second-order time-accurate scheme. Note that these errors are the same order as the errors caused by the first- or second-order approximation of nonlinear parts. In fact, our proposed scheme is an efficient variant of S-SAV method in [20], which retains all advantages of S-SAV method and simplifies the algorithm. To the best of author's knowledge, this is the first work focusing on this variant S-SAV approach for a new modified phase-field surfactant model [20].

The outline of this paper is as follows. We describe the equivalent governing equations in Section 2. We construct the linear, decoupled, and energy stable numerical scheme and analytically prove the discrete energy dissipation law and unique solvability in Section 3. Various computational experiments are presented in Section 4. The conclusions are given in Section 5.

2. Equivalent governing equations

The basic idea of SAV approach [25–27] is to change the original governing equations into equivalent version by using a scalar auxiliary variable, and then construct various linear, energy stable temporal schemes based on the equivalent governing equations. In this study, we define the following auxiliary variable $r(t)$ as

$$r(t) = \int_\Omega \left(F(\phi) + G(\psi) - \frac{\theta}{2}\psi|\nabla\phi|^2 + \frac{\xi}{4}|\nabla\phi|^4\right) d\mathbf{x} + C, \tag{14}$$

where C is a large enough positive constant such that $r(t)$ is positive. Thus, C should satisfy the following relation

$$C > \left[-\int_\Omega \left(F(\phi) + G(\psi) - \frac{\theta}{2}\psi|\nabla\phi|^2 + \frac{\xi}{4}|\nabla\phi|^4\right) d\mathbf{x}\right]_{\max},$$

where the subscript 'max' indicates the maximum value. Because the minimum values of $F(\phi)$, $G(\psi)$, and $\frac{\xi}{4}|\nabla\phi|^4$ are zero, we have

$$C > \left[\int_\Omega \frac{\theta}{2}\psi|\nabla\phi|^2 d\mathbf{x}\right]_{\max}.$$

In the thermodynamical phase-field model [28], the equilibrium profile satisfies $\frac{|\nabla\phi|^2}{2} = \frac{(\phi^2-1)^2}{4\epsilon^2}$. Because the maximum value of ψ is approximately $\psi_s = 1$, we can rewrite the above inequality as follows

$$C > \frac{\theta|\Omega|}{4\epsilon^2}\left[(\phi^2-1)^2\right]_{\max} = \frac{\theta|\Omega|}{4\epsilon^2},$$

where $|\Omega|$ represents the area (volume) of the computational domain in 2D (3D) space. This provides a criterion for choosing the value of C. Practically, $C \geq$ 1e4 is used, which is a large enough value in the most of numerical computations [20,21]. The numerical results in Section 4 indicate this value works well for all simulations. Using $r(t)$, we can rewrite the original energy functional (1) as

$$\mathcal{E}(\phi,\psi,r) = \int_\Omega \left(\frac{\gamma_1}{2}|\nabla\phi|^2 + \frac{\gamma_2}{2}|\nabla\psi|^2\right) d\mathbf{x} + r - C. \tag{15}$$

By taking the variational derivatives of the above equivalent energy with respect to ϕ and ψ, we drive the following equivalent governing equations

$$\phi_t = M_\phi \Delta\mu_\phi, \tag{16}$$
$$\mu_\phi = -\gamma_1\Delta\phi + Pr, \tag{17}$$
$$\psi_t = M_\psi \Delta\mu_\psi, \tag{18}$$
$$\mu_\psi = -\gamma_2\Delta\psi + Qr, \tag{19}$$
$$r_t = \int_\Omega (P\phi_t + Q\psi_t)\, r d\mathbf{x}, \tag{20}$$

where

$$P = \frac{-\xi\nabla\cdot(|\nabla\phi|^2\nabla\phi) + F'(\phi) + \theta\nabla\cdot(\psi\nabla\phi)}{\int_\Omega \left(F(\phi) + G(\psi) - \frac{\theta}{2}\psi|\nabla\phi|^2 + \frac{\xi}{4}|\nabla\phi|^4\right) d\mathbf{x} + C}, \tag{21}$$

$$Q = \frac{G'(\psi) - \frac{\theta}{2}|\nabla\phi|^2}{\int_\Omega \left(F(\phi) + G(\psi) - \frac{\theta}{2}\psi|\nabla\phi|^2 + \frac{\xi}{4}|\nabla\phi|^4\right) d\mathbf{x} + C}. \tag{22}$$

Remarks. We claim Eqs. (16)–(20) are equivalent to Eqs. (8)–(11). We can observe that the numerators in Eqs. (21) and (22) are the nonlinear and coupling terms in Eq. (9) and (11), respectively. The denominator in Eqs. (21) and (22) is the right-hand side of Eq. (14). By using the definition of r in Eq. (14), it is clear that Eqs. (16)–(19) indeed are the original equations, Eqs. (8)–(11). As for the ordinary differential equation, Eq. (20), it can be observed that its solution satisfies the definition of r in Eq. (14) if we take the integral of Eq. (20) with respect to time.

Theorem 2.1. *The equivalent governing Eqs. (16)–(20) satisfy the following energy dissipation law* $\frac{d}{dt}\mathcal{E}(\phi,\psi,r) \leq 0$, *where* $\mathcal{E}(\phi,\psi,r) = \frac{\gamma_1}{2}\|\nabla\phi\|^2 + \frac{\gamma_2}{2}\|\nabla\psi\|^2 + r - C$.

Proof. Taking the L^2-inner product of Eq. (16) with μ_ϕ and using the integration by parts, we have

$$(\phi_t, \mu_\phi) = -M_\phi\|\nabla\mu_\phi\|^2. \tag{23}$$

Taking the L^2-inner product of Eq. (17) with $-\phi_t$, we have

$$-(\phi_t, \mu_\phi) = (\gamma_1\Delta\phi, \phi_t) - (Pr, \phi_t) = -\frac{\gamma_1}{2}\frac{d}{dt}\|\nabla\phi\|^2 - (Pr, \phi_t). \tag{24}$$

Taking the L^2-inner product of Eq. (18) with μ_ψ and using the integration by parts, we have

$$(\psi_t, \mu_\psi) = -M_\psi\|\nabla\mu_\psi\|^2. \tag{25}$$

Taking the L^2-inner product of Eq. (19) with $-\psi_t$, we have

$$-(\psi_t, \mu_\psi) = (\gamma_2\Delta\psi, \psi_t) - (Qr, \psi_t) = -\frac{\gamma_2}{2}\frac{d}{dt}\|\nabla\psi\|^2 - (Qr, \psi_t). \tag{26}$$

From Eq. (20), we have

$$r_t = (Pr, \phi_t) + (Qr, \psi_t). \tag{27}$$

Combining Eqs. (23)–(27) together, we derive

$$\frac{\gamma_1}{2}\frac{d}{dt}\|\nabla\phi\|^2 + \frac{\gamma_2}{2}\frac{d}{dt}\|\nabla\psi\|^2 + r_t = -M_\phi\|\nabla\mu_\phi\|^2 - M_\psi\|\nabla\mu_\psi\|^2 \leq 0, \tag{28}$$

which indicates the equivalent governing equations still satisfy the energy dissipation law.

3. Numerical scheme

In this study, we develop the following linear, temporally second-order accurate, and decoupled numerical scheme for Eqs. (16)–(20) based on the Crank–Nicolson (CN) temporal discretization

$$\frac{\phi^{n+1}-\phi^n}{\Delta t} = M_\phi\Delta\mu_\phi^{n+\frac{1}{2}}, \tag{29}$$
$$\mu_\phi^{n+\frac{1}{2}} = -\gamma_1\left(\frac{\Delta\phi^{n+1}+\Delta\phi^n}{2}\right) + P^*r^* + \frac{S_\phi}{\epsilon^2}\left(\frac{\phi^{n+1}+\phi^n}{2} - \phi^*\right), \tag{30}$$
$$\frac{\psi^{n+1}-\psi^n}{\Delta t} = M_\psi\Delta\mu_\psi^{n+\frac{1}{2}}, \tag{31}$$
$$\mu_\psi^{n+\frac{1}{2}} = -\gamma_2\left(\frac{\Delta\psi^{n+1}+\Delta\psi^n}{2}\right) + Q^*r^* + \frac{S_\psi}{\eta^2}\left(\frac{\psi^{n+1}+\psi^n}{2} - \psi^*\right), \tag{32}$$
$$\frac{r^{n+1}-r^n}{\Delta t} = \int_\Omega \left[P^*r^*\left(\frac{\phi^{n+1}-\phi^n}{\Delta t}\right) + Q^*r^*\left(\frac{\psi^{n+1}-\psi^n}{\Delta t}\right)\right] d\mathbf{x}, \tag{33}$$

where the time step is $\Delta t = T_t/N_t$, T_t and N_t are the total computational time and the number of time iteration, respectively. S_ϕ and S_ψ are positive and constant stabilization coefficients. The superscript " $*$ " represents the explicit extrapolation for the information at $n+\frac{1}{2}$ time level. Here, we will use $\phi^* = \frac{3}{2}\phi^n - \frac{1}{2}\phi^{n-1}$, $\psi^* = \frac{3}{2}\psi^n - \frac{1}{2}\psi^{n-1}$, $P^* = \frac{3}{2}P^n - \frac{1}{2}P^{n-1}$, $Q^* = \frac{3}{2}Q^n - \frac{1}{2}Q^{n-1}$, and $r^* = \frac{3}{2}r^n - \frac{1}{2}r^{n-1}$.

Note that the phase-field function ϕ, surfactant ψ, and auxiliary variable r are decoupled with each other, thus we can first update ϕ^{n+1} from Eqs. (29) and (30), then update ψ^{n+1} from Eqs. (31) and (32). Here, both Eqs. (29)–(30) and Eqs. (31)–(32) are linear and semi-implicit systems with constant coefficients, any fast spatial solver (FFT [29], multigrid [30], etc.) can be used. Finally update r^{n+1} by Eq. (33) in an explicit way. Thus, our algorithm in one time iteration is easy to implement. Because our scheme needs the information at $n-1$ and n time levels, we can use the temporally first-order scheme as the ignition step. Please refer to Appendix for the description of temporally first-order scheme.

Remarks. In this subsection, the temporally second-order accurate and energy stable scheme is designed based on the equivalent Eqs. (16)–(20). In fact, if we want to solve the original Eqs. (8)–(11), the simplest time marching numerical methods are the fully explicit and fully implicit schemes, however it is well known that fully explicit or fully implicit scheme do not satisfy the energy stability due to the existence of nonlinear and coupling terms if a large time step is used. Especially, the coupling term in the last part of Eq. (9) causes difficulties in analysis if one wants to develop a second-order time accurate and unconditionally energy stable scheme. This problem has been reported in previous works [15,17]. Furthermore, the implicit treatment of nonlinear or coupling term will lead to a tedious and coupled system, which makes the numerical computation be complex and costly. Based on the original Eqs. (8)–(11), a linear, decoupled, and temporally second-order scheme can be proposed by using the linear stabilization approach as follows

$$\frac{\phi^{n+1}-\phi^n}{\Delta t} = M_\phi \Delta \mu_\phi^{n+\frac{1}{2}}, \tag{34}$$

$$\mu_\phi^{n+\frac{1}{2}} = -\gamma_1\left(\frac{\Delta\phi^{n+1}+\Delta\phi^n}{2}\right) - \xi\nabla\cdot(|\nabla\phi^*|^2\nabla\phi^*) + F'(\phi^*) + \theta\nabla\cdot(\psi^*\nabla\phi^*) + \frac{S_1}{\epsilon^2}\left(\frac{\phi^{n+1}+\phi^n}{2}-\phi^*\right) \tag{35}$$

$$\frac{\psi^{n+1}-\psi^n}{\Delta t} = M_\psi \Delta \mu_\psi^{n+\frac{1}{2}}, \tag{36}$$

$$\mu_\psi^{n+\frac{1}{2}} = -\gamma_2\left(\frac{\Delta\psi^{n+1}+\Delta\psi^n}{2}\right) + G'(\psi^*) - \frac{\theta}{2}|\nabla\phi^*|^2 + \frac{S_2}{\eta^2}\left(\frac{\psi^{n+1}+\psi^n}{2}-\psi^*\right), \tag{37}$$

where S_1 and S_2 are two positive stabilization coefficients. The above scheme explicitly treats all nonlinear and coupling terms, thus we can efficiently update ϕ^{n+1} and ψ^{n+1} because they are totally decoupled with each other. A similar technique can be found in [31] where the authors used this method to simulate the phase-field dendritic growth model. Although the above scheme seemingly works well at numerical level with the properly chosen values of S_1 and S_2, it still cannot satisfy the unconditionally energy stability due to the existence of nonlinear and coupling terms. In the following simulations, we will not consider the above scheme because this work only focuses on an energy stable method. In the present S-SAV scheme (29)–(33), due to the extra equation, Eq. (33), related to phase-field variables and auxiliary variable, all nonlinear and coupling terms can be eliminated when we perform the energy estimation. Therefore, the unconditional energy stability can be easily proved by using our proposed scheme, some details can be found in Section 3.1. When we update ϕ^{n+1} and ψ^{n+1} by Eqs. (29)–(30) and Eqs. (31)–(32), the total computational cost will be larger than the original equation-based scheme (34)–(37). The equations in both schemes can be thought as linear elliptic equations with constant coefficients. For our proposed scheme, the extra step is to update r^{n+1} by Eq. (33), we note this step needs to calculate the inner products. Moreover, the inner product on the right-hand side of Eq. (14) needs to be updated in each time cycle. Therefore, the total computation may require more time. We numerically validate this in Section 4.3 for a relatively long-time simulation, the results indicate the computational costs introduced by our scheme (29)–(33) and original equation-based scheme (34)–(37) are of the same order.

3.1. Discrete energy dissipation law

Next, we will show that our proposed scheme (16)–(20) satisfies the temporally discrete energy dissipation law by proving the following theorem.

Theorem 3.1. *If ϕ^{n+1}, ϕ^n, ϕ^{n-1}, ψ^{n+1}, ψ^n, ψ^{n-1}, r^{n+1}, and r^n are the solutions of Eqs. (16)–(20), then the following temporally discrete energy dissipation law is satisfied for any time step Δt.*

$$\tilde{\mathcal{E}}(\phi^{n+1},\phi^n,\psi^{n+1},\psi^n,r^{n+1}) \le \tilde{\mathcal{E}}(\phi^n,\phi^{n-1},\psi^n,\psi^{n-1},r^n), \tag{38}$$

where the modified energy functional at n and $n-1$ time levels are defined as

$$\tilde{\mathcal{E}}(\phi^n,\phi^{n-1},\psi^n,\psi^{n-1},r^n) = \frac{\gamma_1}{2}\|\nabla\phi^n\|^2 + \frac{\gamma_2}{2}\|\nabla\psi^n\|^2 + \frac{S_\phi}{4\epsilon^2}\|\phi^n-\phi^{n-1}\|^2 + \frac{S_\psi}{4\eta^2}\|\psi^n-\psi^{n-1}\|^2 + r^n - C. \tag{39}$$

Proof. Taking the L^2-inner product of Eq. (29) with $\Delta t\mu_\phi^{n+\frac{1}{2}}$, we get

$$(\phi^{n+1}-\phi^n) = -\Delta t M_\phi\|\nabla\mu_\phi^{n+\frac{1}{2}}\|^2. \tag{40}$$

Taking the L^2-inner product of Eq. (30) with $-(\phi^{n+1}-\phi^n)$, we obtain

$$-(\mu_\phi^{n+\frac{1}{2}},\phi^{n+1}-\phi^n) = \gamma_1\left(\frac{\Delta\phi^{n+1}+\Delta\phi^n}{2},\phi^{n+1}-\phi^n\right) - (P^*r^*,\phi^{n+1}-\phi^n) - \frac{S_\phi}{\epsilon^2}\left(\frac{\phi^{n+1}+\phi^n}{2}-\phi^*,\phi^{n+1}-\phi^n\right), \tag{41}$$

where

$$\gamma_1\left(\frac{\Delta\phi^{n+1}+\Delta\phi^n}{2},\phi^{n+1}-\phi^n\right) = -\frac{\gamma_1}{2}(\nabla\phi^{n+1}+\nabla\phi^n,\nabla\phi^{n+1}-\nabla\phi^n) = -\frac{\gamma_1}{2}(\|\nabla\phi^{n+1}\|^2-\|\nabla\phi^n\|^2),$$

$$\begin{aligned}
&-\frac{S_\phi}{\epsilon^2}\left(\frac{\phi^{n+1}+\phi^n}{2}-\phi^*,\phi^{n+1}-\phi^n\right)\\
&= -\frac{S_\phi}{\epsilon^2}\left(\frac{\phi^{n+1}+\phi^n}{2}-\left(\frac{3}{2}\phi^n-\frac{1}{2}\phi^{n-1}\right),\phi^{n+1}-\phi^n\right)\\
&= -\frac{S_\phi}{2\epsilon^2}(\phi^{n+1}+\phi^n,\phi^{n+1}-\phi^n) + \frac{S_\phi}{2\epsilon^2}(3\phi^n-\phi^{n-1},\phi^{n+1}-\phi^n)\\
&= -\frac{S_\phi}{2\epsilon^2}(\|\phi^{n+1}\|^2-\|\phi^n\|^2) + \frac{S_\phi}{2\epsilon^2}(\|\phi^{n+1}-\|\phi^n\|^2\\
&-\frac{1}{2}(\|\phi^{n+1}-\phi^n\|^2-\|\phi^n-\phi^{n-1}\|^2+\|\phi^{n+1}-2\phi^n+\phi^{n-1}\|^2))\\
&= -\frac{S_\phi}{4\epsilon^2}(\|\phi^{n+1}-\phi^n\|^2-\|\phi^n-\phi^{n-1}\|^2+\|\phi^{n+1}-2\phi^n+\phi^{n-1}\|^2).
\end{aligned}$$

Therefore, we have

$$-(\mu_\phi^{n+\frac{1}{2}},\phi^{n+1}-\phi^n) = -\frac{S_\phi}{4\epsilon^2}(\|\phi^{n+1}-\phi^n\|^2-\|\phi^n-\phi^{n-1}\|^2+\|\phi^{n+1}-2\phi^n+\phi^{n-1}\|^2) - \frac{\gamma_1}{2}(\|\nabla\phi^{n+1}\|^2-\|\nabla\phi^n\|^2) - (P^*r^*,\phi^{n+1}-\phi^n). \tag{42}$$

Taking the L^2-inner product of Eq. (31) with $\Delta t\mu_\psi^{n+\frac{1}{2}}$, we get

$$(\psi^{n+1}-\psi^n,\mu_\psi^{n+\frac{1}{2}}) = -\Delta t M_\psi\|\nabla\mu_\psi^{n+\frac{1}{2}}\|^2. \tag{43}$$

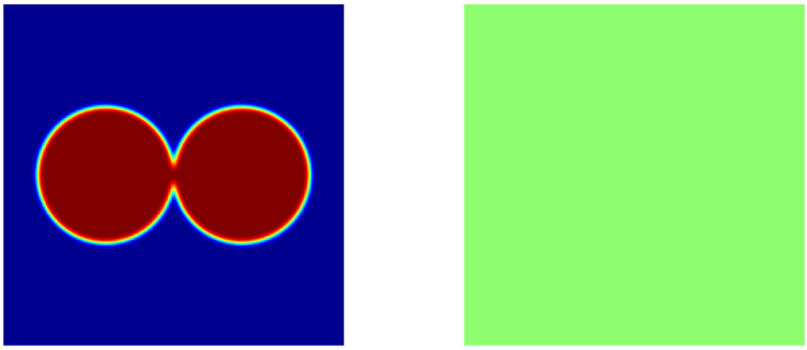

(a) ϕ (b) ψ

Fig. 2. The initial profiles of (a) ϕ and (b) ψ.

Table 1
L^2-errors and convergence rates of ϕ and ψ (data in parentheses bracket) with different time steps. The numerical reference is obtained with $\Delta t^r = 2.4096\text{e-}5$ at $t = 0.03$.

Δt	$4\Delta t^r$		$8\Delta t^r$		$16\Delta t^r$		$32\Delta t^r$		$64\Delta t^r$
$S = 0$:	8.11e-8 (1.97e-8)		3.41e-7 (8.31e-8)		1.38e-6 (3.39e-7)		5.56e-6 (1.38e-6)		7.90e-4 (4.10e-2)
Rate		2.07 (2.08)		2.02 (2.03)		2.01 (2.03)		7.15 (14.86)	
$S = 2$:	2.67e-7 (7.90e-9)		1.08e-6 (3.53e-8)		4.35e-6 (1.46e-7)		1.75e-5 (6.01e-7)		7.06e-5 (4.58e-6)
Rate		2.02 (2.016)		2.01 (2.06)		2.01 (2.04)		2.01 (2.93)	
$S = 6$:	6.63e-7 (2.19e-8)		2.67e-6 (8.42e-8)		1.07e-5 (3.35e-7)		4.30e-5 (1.34e-6)		1.74e-4 (5.44e-6)
Rate		2.01 (1.95)		2.00 (1.99)		2.01 (2.00)		2.02 (2.02)	
$S = 10$:	1.06e-6 (4.81e-8)		4.26e-6 (1.89e-7)		1.71e-5 (7.57e-7)		6.88e-5 (3.05e-6)		2.80e-4 (1.25e-5)
Rate		2.01 (1.98)		2.00 (2.00)		2.01 (2.01)		2.03 (2.03)	

Taking the L^2-inner product of Eq. (32) with $-(\psi^{n+1} - \psi^n)$, we obtain

$$-(\mu_\psi^{n+\frac{1}{2}}, \psi^{n+1} - \psi^n) = \gamma_2 \left(\frac{\Delta\psi^{n+1} + \Delta\psi^n}{2}, \psi^{n+1} - \psi^n \right) - (Q^* r^*, \psi^{n+1} - \psi^n) - \frac{S_\psi}{\eta^2} \left(\frac{\psi^{n+1} + \psi^n}{2} - \psi^*, \psi^{n+1} - \psi^n \right), \quad (44)$$

where

$$\begin{aligned}
&\gamma_2 \left(\frac{\Delta\psi^{n+1} + \Delta\psi^n}{2}, \psi^{n+1} - \psi^n \right) \\
&= -\frac{\gamma_2}{2} (\nabla\psi^{n+1} + \nabla\psi^n, \nabla\psi^{n+1} - \nabla\psi^n) \\
&= -\frac{\gamma_2}{2} (\|\nabla\psi^{n+1}\|^2 - \|\nabla\psi^n\|^2),
\end{aligned}$$

$$\begin{aligned}
&-\frac{S_\psi}{\eta^2} \left(\frac{\psi^{n+1} + \psi^n}{2} - \psi^*, \psi^{n+1} - \psi^n \right) \\
&= -\frac{S_\psi}{\eta^2} \left(\frac{\psi^{n+1} + \psi^n}{2} - \left(\frac{3}{2}\psi^n - \frac{1}{2}\psi^{n-1} \right), \psi^{n+1} - \psi^n \right) \\
&= -\frac{S_\psi}{2\eta^2} (\psi^{n+1} + \psi^n, \psi^{n+1} - \psi^n) + \frac{S_\psi}{2\eta^2} (3\psi^n - \psi^{n-1}, \psi^{n+1} - \psi^n) \\
&= -\frac{S_\psi}{2\eta^2} (\|\psi^{n+1}\|^2 - \|\psi^n\|^2) + \frac{S_\psi}{2\eta^2} (\|\psi^{n+1} - \|\psi^n\|^2 \\
&- \frac{1}{2} (\|\psi^{n+1} - \psi^n\|^2 - \|\psi^n - \psi^{n-1}\|^2 + \|\psi^{n+1} - 2\psi^n + \psi^{n-1}\|^2)) \\
&= -\frac{S_\psi}{4\eta^2} (\|\psi^{n+1} - \psi^n\|^2 - \|\psi^n - \psi^{n-1}\|^2 + \|\psi^{n+1} - 2\psi^n + \psi^{n-1}\|^2).
\end{aligned}$$

Therefore, we obtain

$$\begin{aligned}
-(\mu_\psi^{n+\frac{1}{2}}, \psi^{n+1} - \psi^n) = &-\frac{S_\psi}{4\eta^2} (\|\psi^{n+1} - \psi^n\|^2 - \|\psi^n - \psi^{n-1}\|^2 \\
&+ \|\psi^{n+1} - 2\psi^n + \psi^{n-1}\|^2) \\
&- \frac{\gamma_2}{2} (\|\nabla\psi^{n+1}\|^2 - \|\nabla\psi^n\|^2) \\
&- (Q^* r^*, \psi^{n+1} - \psi^n). \quad (45)
\end{aligned}$$

From Eq. (33), we have

$$r^{n+1} - r^n = (P^* r^*, \phi^{n+1} - \phi^n) + (Q^* r^*, \psi^{n+1} - \psi^n). \quad (46)$$

Combining Eqs. (40), (42), (43), (45), and (46) together, we can derive that

$$\begin{aligned}
&r^{n+1} - r^n + \frac{\gamma_1}{2} (\|\nabla\phi^{n+1}\|^2 - \|\nabla\phi^n\|^2) \\
&\quad + \frac{\gamma_2}{2} (\|\nabla\psi^{n+1}\|^2 - \|\nabla\psi^n\|^2) \\
&+ \frac{S_\phi}{4\epsilon^2} (\|\phi^{n+1} - \phi^n\|^2 - \|\phi^n - \phi^{n-1}\|^2 + \|\phi^{n+1} - 2\phi^n + \phi^{n-1}\|^2) \\
&+ \frac{S_\psi}{4\eta^2} (\|\psi^{n+1} - \psi^n\|^2 - \|\psi^n - \psi^{n-1}\|^2 \\
&\quad + \|\psi^{n+1} - 2\psi^n + \psi^{n-1}\|^2) \\
&= -\Delta t M_\phi \|\nabla\mu_\phi^{n+\frac{1}{2}}\|^2 - \Delta t M_\psi \|\nabla\mu_\psi^{n+\frac{1}{2}}\|^2 \le 0. \quad (47)
\end{aligned}$$

The proof is completed.

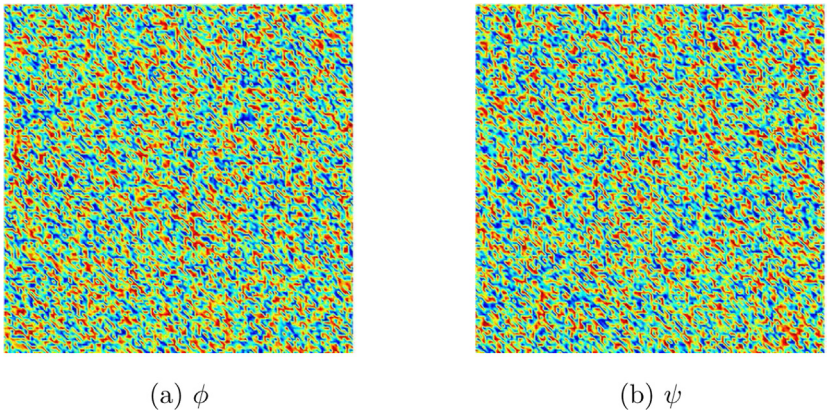

Fig. 3. The initial profiles of (a) ϕ and (b) ψ.

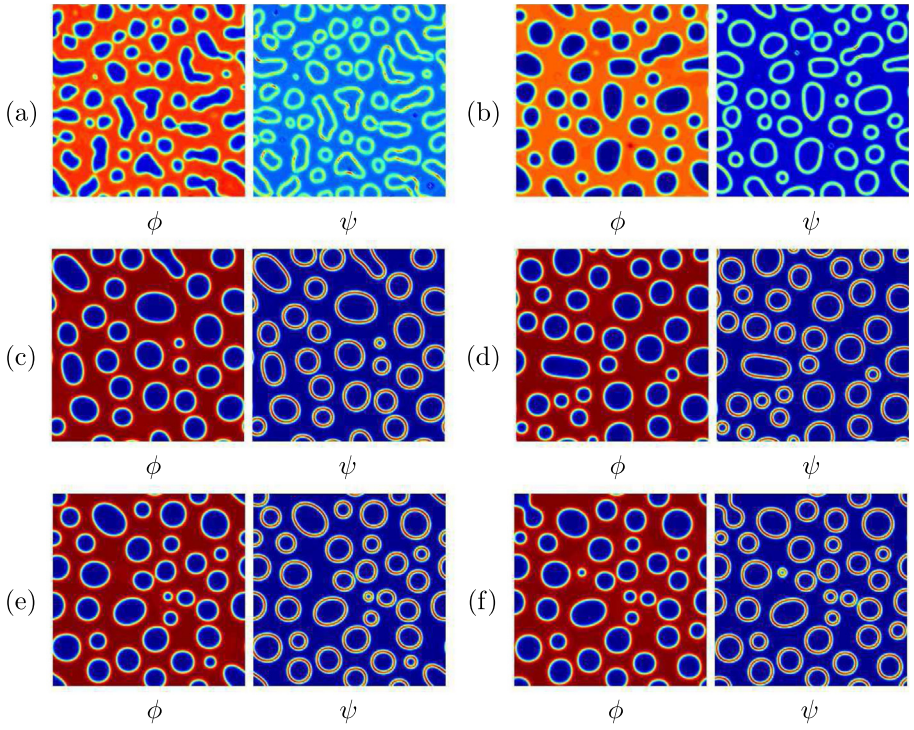

Fig. 4. Snapshots of ϕ and ψ at $t = 40$ with respect to different time steps. The time steps are $\Delta t = 1,\ 0.5,\ 0.1,\ 0.05,\ 0.01$, and 0.001 with respect to (a)–(f), respectively.

3.2. Unique solvability

In this part, we will prove our proposed scheme admits unique solution pairs $(\phi^{n+1}, \mu_\phi^{n+\frac{1}{2}})$ and $(\psi^{n+1}, \mu_\psi^{n+\frac{1}{2}})$. Because the variables ϕ, ψ, and r are decoupled in one time iteration, we can prove them separately. We first focus on the proof for ϕ. Taking the L^2-inner product of Eq. (29) with $\mathbf{1}$, we get

$$\int_\Omega \phi^{n+1} d\mathbf{x} = \int_\Omega \phi^n d\mathbf{x} = \cdots = \int_\Omega \phi^0 d\mathbf{x}. \tag{48}$$

Let $V_\phi = \frac{1}{|\Omega|}\int_\Omega \phi^0 d\mathbf{x}$ and $V_\mu = \frac{1}{\Omega}\int_\Omega \mu_\phi^{n+\frac{1}{2}} d\mathbf{x}$ be the mean values, then we define

$$\hat{\phi}^{n+1} = \phi^{n+1} - V_\phi, \quad \hat{\mu_\phi}^{n+\frac{1}{2}} = \mu_\phi^{n+\frac{1}{2}} - V_\mu, \tag{49}$$

where $(\hat{\phi}^{n+1}, \hat{\mu_\phi}^{n+\frac{1}{2}})$ are the solutions of the following equations with unknowns (ϕ, μ_ϕ)

$$\frac{1}{M_\phi \Delta t}\phi - \Delta \mu_\phi = f, \tag{50}$$

$$\mu_\phi + V_\mu + \frac{\gamma_1}{2}\Delta\phi - \frac{S_\phi}{2\epsilon^2}\phi = g, \tag{51}$$

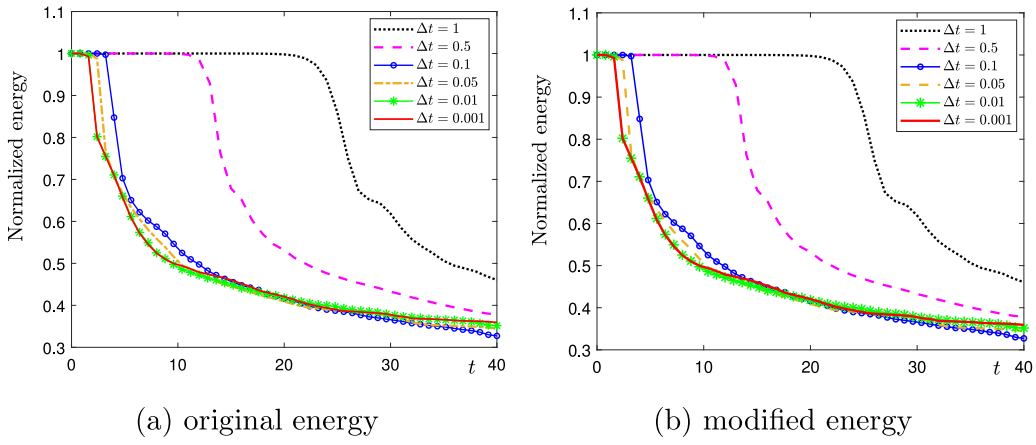

Fig. 5. Temporal evolutions of normalized (a) original energy functional and (b) modified energy functional with respect to different time steps.

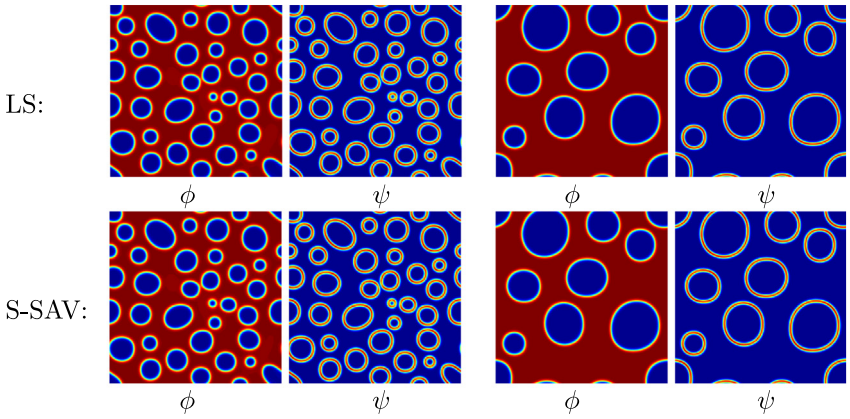

Fig. 6. The profiles of ϕ and ψ obtained by the LS and the S-SAV approaches. The left and right subfigures are at $t = 4$ and 40.

where $f = \frac{1}{M_\phi \Delta t}\hat{\phi}^n$ and $g = P^* r^* - \frac{S_\phi}{2\epsilon^2}\hat{\phi}^n - \frac{\gamma_1}{2}\Delta\phi^n - \frac{S_\phi}{\epsilon^2}\phi^*$. For a mean zero variable ν, we can define the following inverse Laplacian operation

$$\tilde{\nu} := \Delta^{-1}\nu, \quad \Delta\tilde{\nu} = \nu, \tag{52}$$

where $\tilde{\nu}$ is mean zero. Here, the periodic or zero-Neumann boundary conditions will be used. By applying $-\Delta^{-1}$ to Eq. (50) and using Eq. (51), we obtain

$$-\frac{1}{M_\phi \Delta t}\Delta^{-1}\phi - V_\mu - \frac{\gamma_1}{2}\Delta\phi + \frac{S_\phi}{2\epsilon^2}\phi = -\Delta^{-1}f - g. \tag{53}$$

The above linear system can be recast to be $A(\phi) = b$. For any variables ϕ_1 and ϕ_2 satisfying the mean zero condition and proper boundary condition, we get

$$\begin{aligned}(A(\phi_1), \phi_2) &= -\frac{1}{M_\phi \Delta t}(\Delta^{-1}\phi_1, \phi_2) + \left(\frac{S_\phi}{2\epsilon^2}\phi_1 - \frac{\gamma_1}{2}\Delta\phi_1, \phi_2\right) \\ &\le B_1(\|\nabla\Delta^{-1}\phi_1\| \cdot \|\nabla\Delta^{-1}\phi_2\| + \|\nabla\phi_1\| \cdot \|\nabla\phi_2\| \\ &\quad + \|\phi_1\| \cdot \|\phi_2\|) \\ &\le B_2\|\phi_1\|_{H^1} \cdot \|\phi_2\|_{H^1}, \end{aligned} \tag{54}$$

where B_1 and B_2 are constants that depend on parameters Δt, M_ϕ, S_ϕ, ϵ, and γ_1, etc. The notation $\|\cdot\|_{H^1}$ is the $H^1(\Omega)$ norm. We find the bilinear form $(A(\phi_1), \phi_2)$ is bounded for any ϕ_1 and ϕ_2 in $H^1(\Omega)$. For any variable ϕ satisfying mean zero condition, we have

$$(A(\phi), \phi) = \frac{1}{M_\phi \Delta t}\|\nabla\Delta^{-1}\phi\|^2 + \frac{\gamma_1}{2}\|\nabla\phi\|^2 + \frac{S_\phi}{2\epsilon^2}\|\phi\|^2 \ge B_3\|\phi\|_{H^1}^2, \tag{55}$$

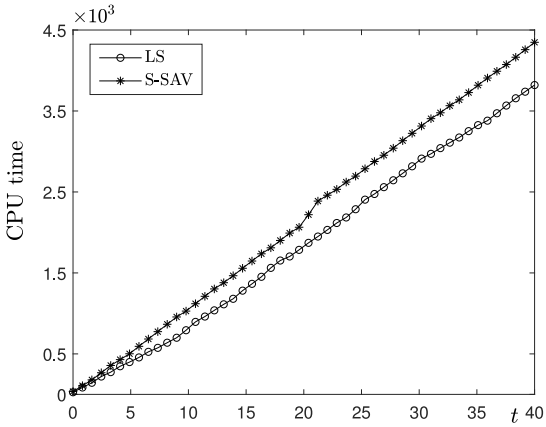

Fig. 7. Computational costs required by the LS and the S-SAV approaches.

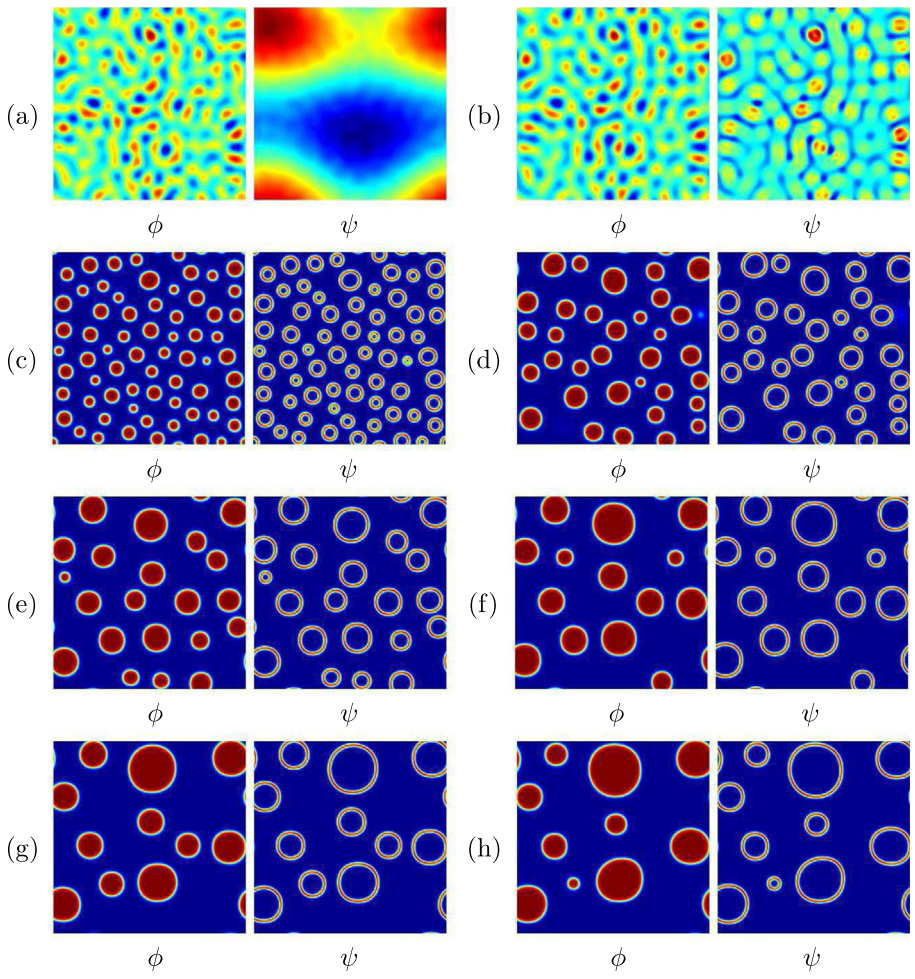

Fig. 8. Temporal evolution of phase separation with $\bar{\phi} = -0.5$. The subfigures (a)–(h) are at $t = 0.4,\ 1,\ 2,\ 4,\ 10,\ 20,\ 30,\ 40$.

where B_3 is a constant that depends on some parameters Δt, M_ϕ, S_ϕ, ϵ, and γ_1, etc. Therefore, the bilinear form is coercive. By using the Lax–Milgram theorem, we conclude that Eqs. (50) and (51) admit a unique solution in $H^1(\Omega)$. Moreover, we also find that $(A(\phi_1), \phi_2) = (\phi_1, A(\phi_2))$, which means A is self-adjoint. From Eq. (55), it is easy to find that $(A(\phi), \phi) \geq 0$, where " $=$ " holds if and only if $\phi = 0$. We can conclude that the linear operator A is positive definite. Now, we have proved the existence of unique solution for Eqs. (29)–(30). Note that the same process can be directly used to prove the unique solvability of Eqs. (31)–(32) for ψ, we will omit them and leave those similar steps to interested readers. After ϕ and ψ are known, r can be directly updated by Eq. (33) in an explicit manner, its unique solvability is obvious.

Remarks. In this section, we can observe that the main contributions of auxiliary variable r are at numerical computation and energy stable analysis: (i) Based on the equivalent equations, we can treat all nonlinear and coupling terms in an explicit way, thus the numerical scheme is linear, decoupled and very easy to implement. (ii) Adding an auxiliary variable leads to an extra governing equation. By using this extra equation related to phase-field variables and auxiliary variable, the unconditionally energy stability of the whole system can be easily established because all nonlinear and coupling terms are eliminated in the proof.

4. Numerical experiments

In this work, we only focus on an efficient temporal scheme for a new modified phase-field surfactant model [20]. The spatial discretization is based on the standard finite difference formulation. Efficient linear multigrid algorithm is used for solving the discrete system. Please refer to [30] for some details of multigrid method. All tests are conducted on the two-dimensional domain $\Omega^2 = [0, 2\pi]^2$ or the three-dimensional domain $\Omega^3 = [0, 2\pi]^3$ with mesh size $h = \pi/64$. The periodic boundary condition and the following parameters: $\gamma_1 = \gamma_2 = 1$, $M_\phi = M_\psi = 0.0001$, $\epsilon = 0.04$, $\eta = 0.04$, $\theta = 0.5$, $\xi = 0.001$, $\psi_s = 1$, $C = 1e6$ are used without specific needs.

4.1. Accuracy test

To numerically verify the temporally second-order accuracy of our scheme, we consider the following initial conditions

$$\phi(x, y, 0) = \tanh\left(\frac{0.4\pi - \sqrt{(x - 0.6\pi)^2 + (y - \pi)^2}}{\sqrt{2}\epsilon}\right) + \tanh\left(\frac{0.4\pi - \sqrt{(x - 1.4\pi)^2 + (y - \pi)^2}}{\sqrt{2}\epsilon}\right) + 1, \quad (56)$$

$$\psi(x, y, 0) = 0.3. \quad (57)$$

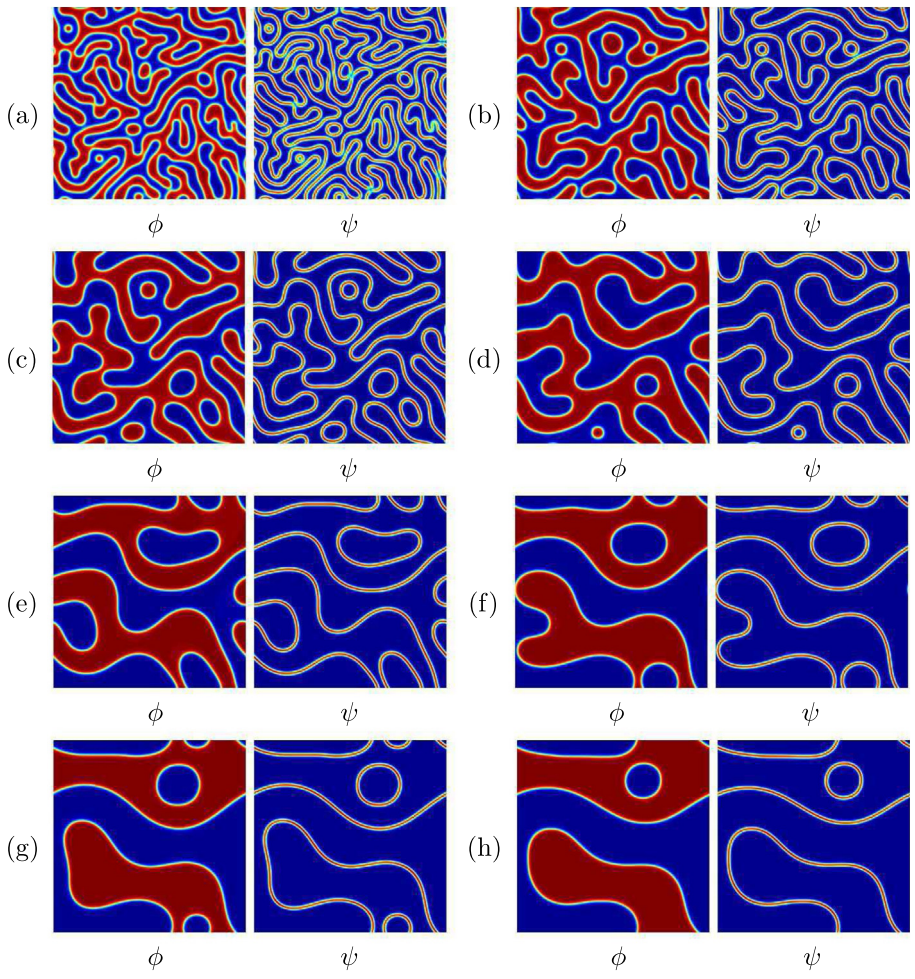

Fig. 9. Temporal evolution of phase separation with $\bar{\phi} = 0$. The subfigures (a)–(h) are at $t = 0.4,\ 1,\ 2,\ 4,\ 10,\ 20,\ 30,\ 40$.

Table 2
L^2-errors and convergence rates of ϕ and ψ with different time steps. The numerical reference is obtained with $\Delta t^r = 0.001$ at $t = 1.28$. Here, $S = 6$ is used.

Δt	ϕ	Rate	ψ	Rate
$128\Delta t^r$	1.18e−1	–	1.80e−3	–
$64\Delta t^r$	3.13e−2	1.88	4.81e−4	1.90
$32\Delta t^r$	7.50e−3	2.06	1.15e−4	2.06
$16\Delta t^r$	1.90e−3	1.98	2.96e−5	1.96
$8\Delta t^r$	4.83e−4	1.98	7.39e−6	2.00
$4\Delta t^r$	1.15e−4	2.07	1.76e−6	2.07

Table 3
L^2-errors and convergence rates of ϕ and ψ with different time steps. The numerical reference is obtained with $\Delta t^r = 0.001$ at $t = 1.28$. Here, $S = 10$ is used.

Δt	ϕ	Rate	ψ	Rate
$128\Delta t^r$	1.53e−1	–	2.80e−3	–
$64\Delta t^r$	5.38e−2	1.51	8.60e−4	1.70
$32\Delta t^r$	1.20e−2	2.16	1.87e−4	2.20
$16\Delta t^r$	3.10e−3	1.95	4.75e−5	1.97
$8\Delta t^r$	7.82e−4	1.99	1.20e−5	1.99
$4\Delta t^r$	1.90e−4	2.04	2.91e−6	2.04

Figs. 2(a) and (b) show the initial profiles of ψ and ψ, respectively. A series of different stabilization coefficients: $S_\phi = S_\psi = 0,\ 2,\ 6$, and 10 are used to study the effects of S_ϕ and S_ψ. Since S_ϕ and S_ψ take the same value in this work, we will use S for convenience. At first, we define the reference result as the solution obtained by a small enough time step $\Delta t^f = 0.01h^2 \approx 2.4096\text{e-}5$. Table 1 illustrates the L^2-errors and convergence rates [32] of ϕ and ψ at $t = 0.03$ with respect to different stabilization coefficients. As we can observe, the case with $S = 0$ does not satisfy the second-order accuracy with a larger time step; the case $S = 2$ violates the desired accuracy for ψ with a larger time step; the cases $S = 6$ and $S = 10$ satisfy the desired accuracy.

To choose more proper stabilization coefficients, we consider $S = 6$ and 10 with some large time steps. Here, the reference result is obtained by the time step $\Delta t^f = 0.001$. The L^2-errors and convergence rates of ϕ and ψ at $t = 1.28$ are shown in Tables 2 and 3. We can find that the case $S = 10$ slightly loses some accuracy at a larger time step. In the case $S = 6$, the desired second-order accuracy is satisfied even if larger time steps are used. In the following tests, we will use the proper stabilization coefficient $S = 6$.

4.2. Energy dissipation law

The energy dissipation law is a fundamental property of the phase-field surfactant model. To verify the discrete energy dissipation law of our scheme, we consider the phase separation with

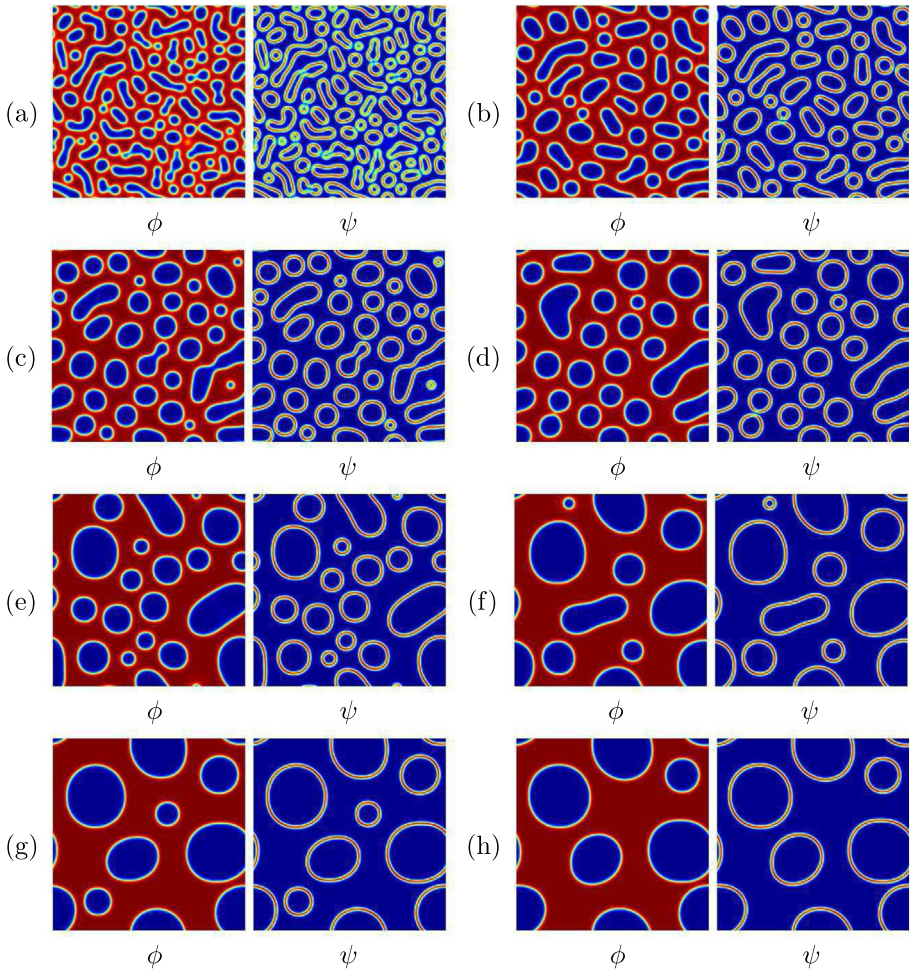

Fig. 10. Temporal evolution of phase separation with $\bar{\phi} = 0.2$. The subfigures (a)–(h) are at $t = 0.4,\ 1,\ 2,\ 4,\ 10,\ 20,\ 30,\ 40$.

the following initial conditions

$$\phi(x, y, 0) = 0.3 + 0.0001\text{rand}(x, y), \tag{58}$$

$$\psi(x, y, 0) = 0.2 + 0.0001\text{rand}(x, y), \tag{59}$$

where rand(x,y) is the random number between -1 and 1. Figs. 3(a) and (b) show the initial profiles of ϕ and ψ, respectively. A series of increasing large time steps: $\Delta t = 0.001,\ 0.01,\ 0.05,\ 0.1,\ 0.5$, and 1 are used. The snapshots at $t = 40$ with respect to different time steps are displayed in Fig. 4. The temporal evolutions of normalized original energy functional $\mathcal{E}(\phi^n, \psi^n)/\mathcal{E}(\phi^0, \psi^0)$ and normalized modified energy functional $\tilde{\mathcal{E}}(\phi^n, \phi^{n-1}, \psi^n, \psi^{n-1}, r^n)/\tilde{\mathcal{E}}(\phi^0, \psi^0, r^0)$ are shown in Figs. 5(a) and (b). We find that the discrete energy dissipation law is satisfied even if larger time steps are used. In actual simulation, a smaller time step is necessary. Furthermore, the evolutions of original energy and modified energy are very similar, which indicates the modified energy functional is a proper approximation of original energy functional.

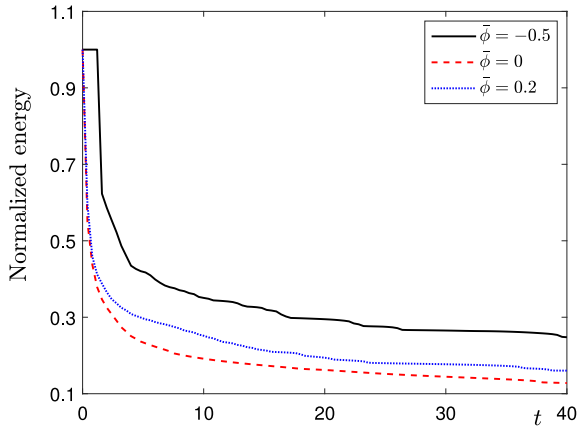

Fig. 11. Temporal evolutions of normalized energy functional with respect to different $\bar{\phi}$.

4.3. Comparison with the linear stabilization approach

As mentioned in Section 3, our propose scheme (29)–(33) (S-SAV) may require more computational cost than the original equation-based scheme (34)–(37) (LS) because of the extra computations for inner products. To numerically validate this, we use the same initial conditions and parameters in Section 4.2. The relatively long-time simulations until $t = 40$ are considered. Fig. 6 illustrates the profiles of ϕ and ψ at specific moments. Although the S-SAV approach is designed based on the equivalent equations instead of the original equations, it can be observed that the results obtained by the S-SAV approach and the original equation-based LS approach are almost same. We list the CPU time required by two schemes in Fig. 7, the results indicate that our proposed scheme requires extra 13.78% CPU cost than the original equation-based LS approach.

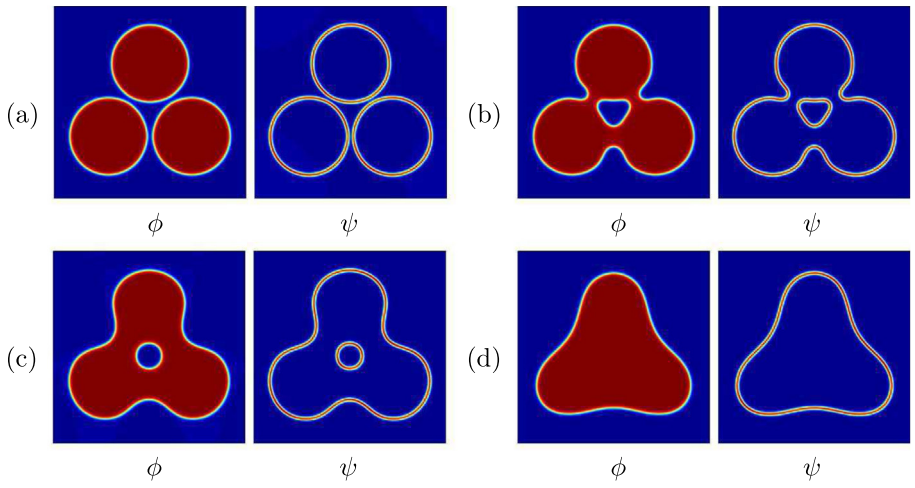

Fig. 12. Temporal evolution of three droplets with $\theta = 0.01$. The subfigures (a)–(d) are at $t = 1,\ 4,\ 10,\ 20$.

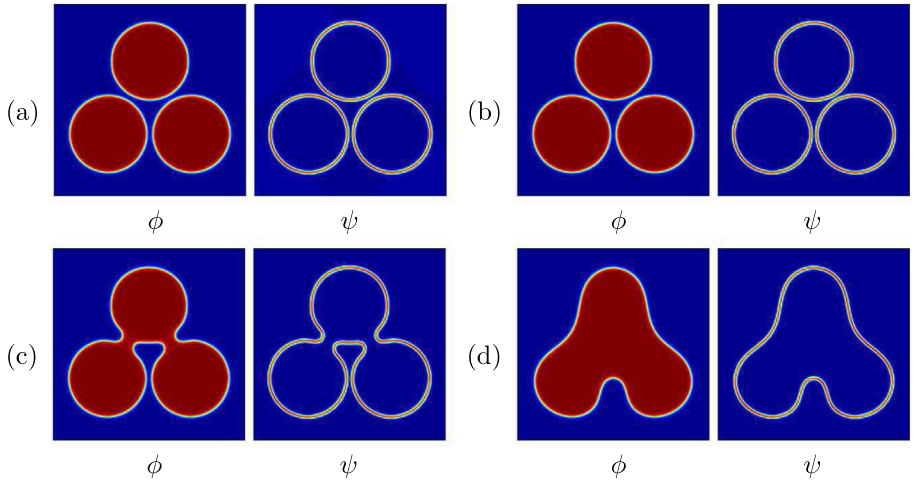

Fig. 13. Temporal evolution of three droplets with $\theta = 1$. The subfigures (a)–(d) are at $t = 1,\ 4,\ 10,\ 20$.

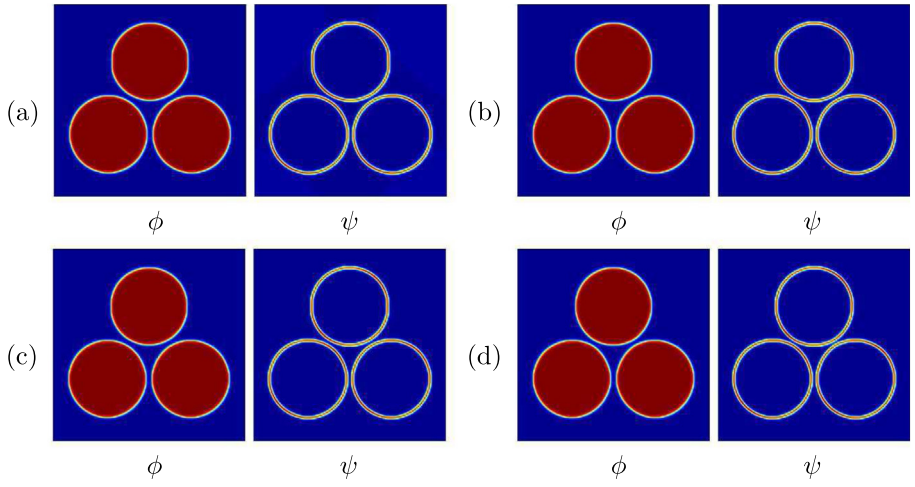

Fig. 14. Temporal evolution of three droplets with $\theta = 2$. The subfigures (a)–(d) are at $t = 1,\ 4,\ 10,\ 20$.

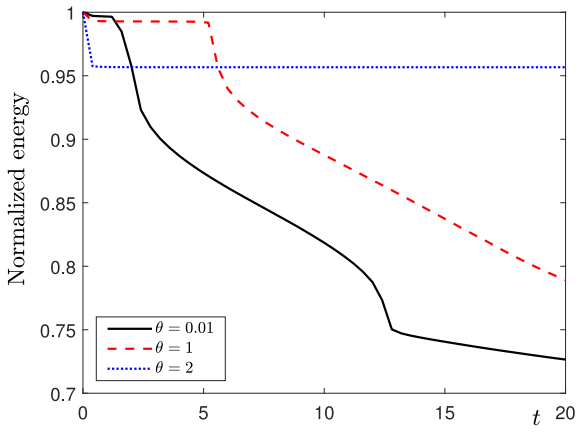

Fig. 15. Temporal evolutions of normalized energy functional with respect to different θ.

4.4. Two-dimensional phase separation

In this section, we investigate the phase separation in two-dimensional space, which is a typical benchmark problem of the Cahn–Hilliard type model. The following initial conditions are considered

$$\phi(x, y, 0) = \bar{\phi} + 0.001\text{rand}(x, y), \tag{60}$$
$$\psi(x, y, 0) = 0.2 + 0.001\text{rand}(x, y), \tag{61}$$

where $\bar{\phi} = -0.5,\ 0$, and 0.2 are used to generate different evolutional patterns. Here, $\Delta t = 0.001$ is used and all simulations are performed until $t = 40$. From Figs. 8–10, we find $\bar{\phi} = 0$ means two immiscible mixtures always occupy same concentration during the evolution. With the increase of absolute value of ϕ, we can find the mixture with lower concentration evolves to form some isolated parts, the mixture with higher concentration occupies main regions. In all cases, the local concentration of ψ always accumulates on the interface. We plot the normalized energy curves with respect to various values of $\bar{\phi}$ in Fig. 11. As we can see, the discrete energy dissipation law is satisfied.

4.5. Effect of θ

Next, we numerically show the effect of θ on the interfacial dynamics. The initial conditions are defined as

$$\begin{aligned}\phi(x, y, 0) = &\tanh\left(\frac{0.4\pi - \sqrt{(x-0.57\pi)^2 + (y-0.65\pi)^2}}{\sqrt{2}\epsilon}\right)\\ &+ \tanh\left(\frac{0.4\pi - \sqrt{(x-1.43\pi)^2 + (y-0.65\pi)^2}}{\sqrt{2}\epsilon}\right)\\ &+ \tanh\left(\frac{0.4\pi - \sqrt{(x-\pi)^2 + (y-1.4\pi)^2}}{\sqrt{2}\epsilon}\right) + 2,\end{aligned} \tag{62}$$

$$\psi(x, y, 0) = 0.2 + 0.001\text{rand}(x, y). \tag{63}$$

Here, $\Delta t = 0.001$ is used. In free energy formula, Eq. (4), the θ represents the strength of the coupling between ϕ and ψ. For a surfactant-laden two-phase system, it is well known that the surfactant can be used to affect the interfacial dynamics by changing the surface tension. In the simulation, a smaller value of θ means the effect of surfactant is weak, then the strong interfacial tension will drive the interfaces to coalesce with each other. On the other hand, a larger value of θ increases the effect of surfactant, then three droplets will keep separated for a long time. Fig. 12 presents the temporal evolution with $\theta = 0.01$. We can find the three droplets quickly merge into a big one. Fig. 13 illustrates the evolution with $\theta = 1$, we find that a larger value of θ obviously delays the interfacial dynamics. In Fig. 14, we plot the results with $\theta = 2$. We observe a large enough value of θ overcomes the coarsening effect of interface, the three droplets keep separated all long. Fig. 15 shows the evolutions of discrete normalized energy with respect to three values of θ, the results indicate the discrete energy dissipation law is satisfied.

4.6. Three-dimensional phase separation

Finally, we investigate the phase separation in three-dimensional space. The following initial conditions are used

$$\phi(x, y, z, 0) = \bar{\phi} + 0.001\text{rand}(x, y, z), \tag{64}$$
$$\psi(x, y, z, 0) = 0.2 + 0.001\text{rand}(x, y, z). \tag{65}$$

Here, we only consider two typical cases, i.e., $\bar{\phi} = 0$, and 0.3. The parameters $\Delta t = 0.001$, $\epsilon = \eta = 0.06$ are used. Figs. 16(a) and (b) show the initial profiles of ϕ and ψ, respectively. We display the temporal evolutions of ϕ and ψ in Figs. 17 and 18 with respect to $\bar{\phi} = 0$ and 0.3, respectively. We can see that different values of average concentration leads to different evolutional dynamics. The local concentration of ψ always accumulates on the interface. Fig. 19 shows the normalized energy curves with respect to $\bar{\phi} = 0$ and 0.3. The results indicate that the discrete energy dissipation law is satisfied in three-dimensional space.

5. Conclusions

In this study, we constructed a linear, decoupled, second-order accurate, and energy stable numerical scheme for a new modified phase-field surfactant model. As an efficient variant of S-SAV approach, our scheme inherited all advantages of S-SAV method but significantly simplified the algorithm. In the present version, the phase-field function, surfactant, and auxiliary variable were decoupled with each other. Thus, we could solve them in a step-by-step way. Energy stability and unique solvability of our proposed scheme were analytically proved. Various numerical results showed that the proposed scheme had desired accuracy and energy stability. In upcoming work, we will investigate the hydrodynamically coupled phase-field surfactant model by using our proposed scheme. To construct energy stable phase-field system with fluid flow, please refer to some previous works [33,34].

Declaration of competing interest

The authors declare that they have no known competing financial interests or personal relationships that could have appeared to influence the work reported in this paper.

Acknowledgments

J. Yang is supported by China Scholarship Council (201908260060). The corresponding author (J.S. Kim) was supported by Basic Science Research Program through the National Research Foundation of Korea (NRF) funded by the Ministry of Education, South Korea (NRF-2019R1A2C1003053). The authors appreciate the reviewers for their constructive comments, which have improved the quality of this paper.

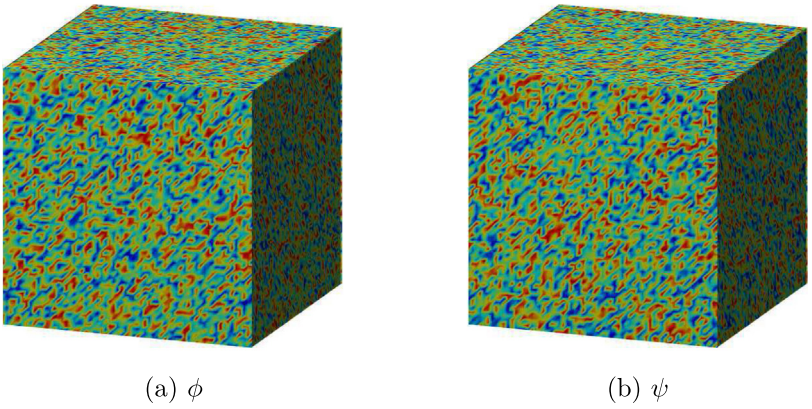

Fig. 16. The initial profiles of (a) ϕ and (b) ψ in 3D space.

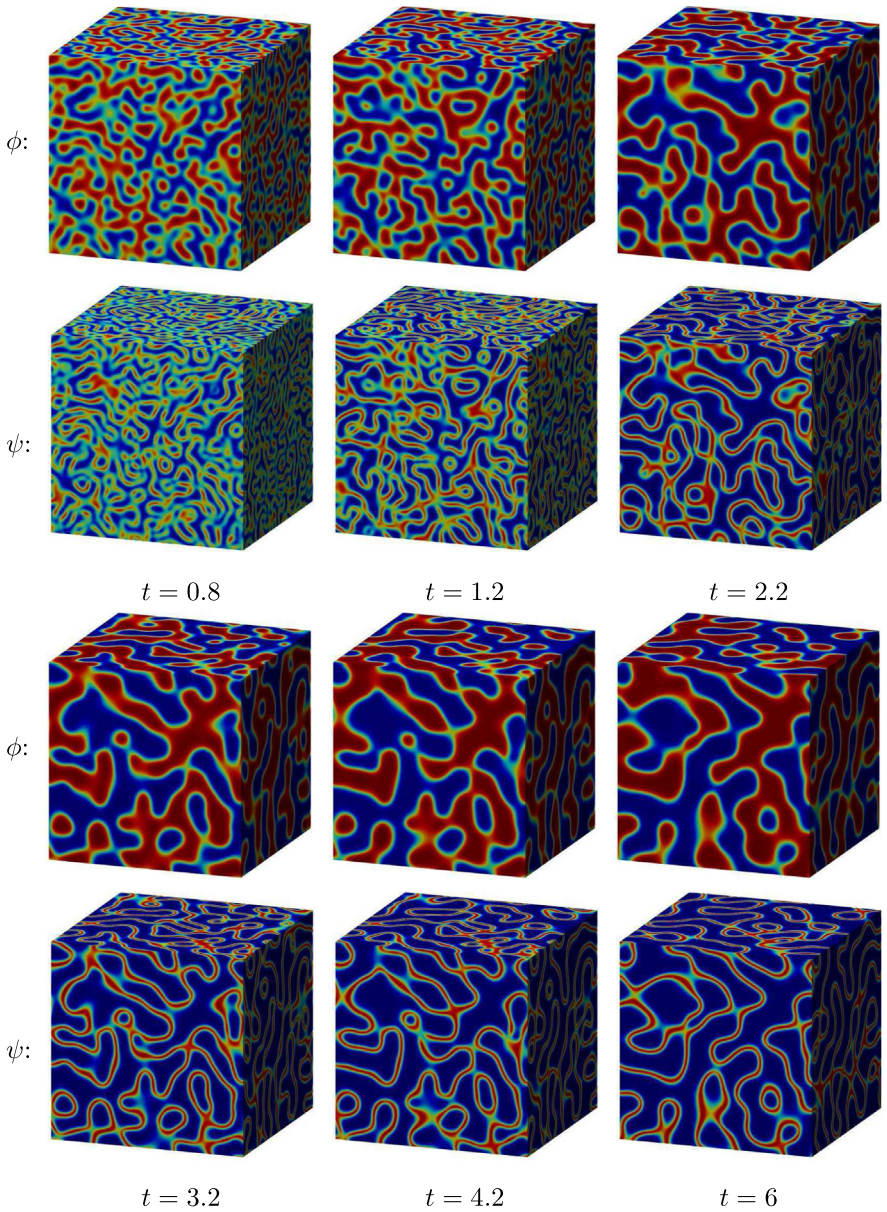

Fig. 17. Temporal evolution of three-dimensional phase separation with $\bar{\phi} = 0$.

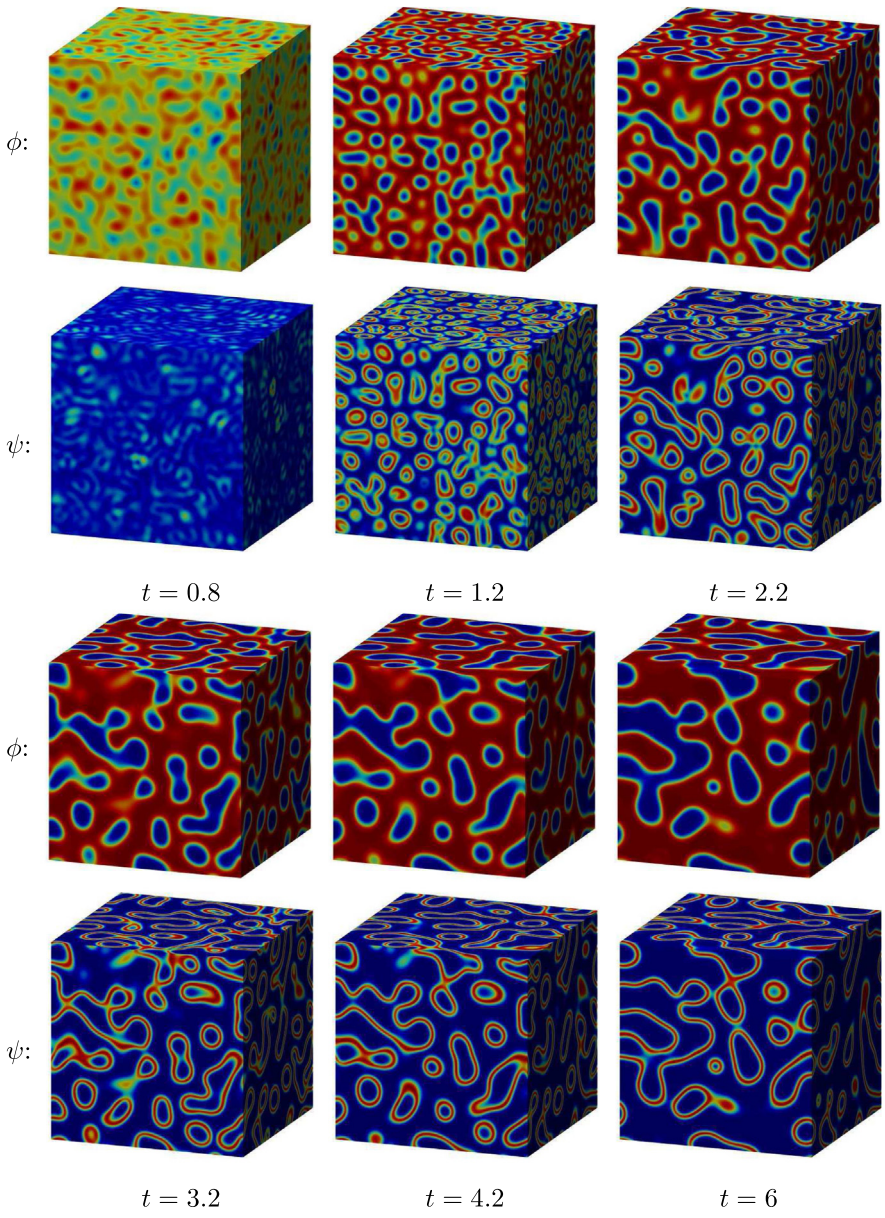

Fig. 18. Temporal evolution of three-dimensional phase separation with $\bar{\phi} = 0.3$.

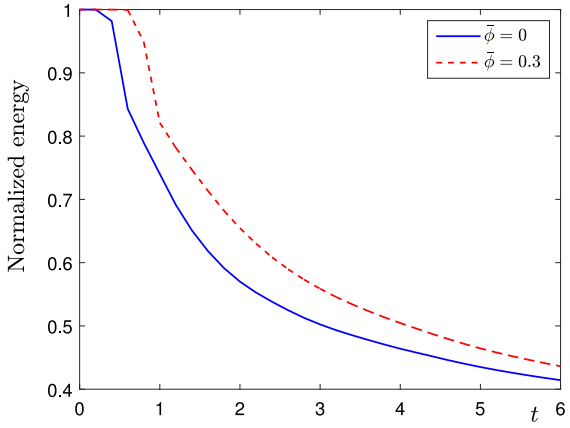

Fig. 19. Temporal evolutions of normalized energy functional with respect to different $\bar{\phi}$.

Appendix

Here, we introduce the temporally first-order scheme by using our proposed method. The first-order scheme is constructed based on the backward-Euler formulation

$$\frac{\phi^{n+1} - \phi^n}{\Delta t} = M_\phi \Delta \mu_\phi^{n+1}, \tag{66}$$

$$\mu_\phi^{n+1} = -\gamma_1 \Delta \phi^{n+1} + P^n r^n + \frac{S_\phi}{\epsilon^2}(\phi^{n+1} - \phi^n), \tag{67}$$

$$\frac{\psi^{n+1} - \psi^n}{\Delta t} = M_\psi \Delta \mu_\psi^{n+1}, \tag{68}$$

$$\mu_\psi^{n+1} = -\gamma_2 \Delta \psi^{n+1} + Q^n r^n + \frac{S_\psi}{\eta^2}(\psi^{n+1} - \psi^n), \tag{69}$$

$$\frac{r^{n+1} - r^n}{\Delta t} = \int_\Omega \left[P^n r^n \left(\frac{\phi^{n+1} - \phi^n}{\Delta t} \right) + Q^n r^n \left(\frac{\psi^{n+1} - \psi^n}{\Delta t} \right) \right] d\mathbf{x}. \tag{70}$$

Next, we will show the discrete energy dissipation law by proving the following theorem.

Theorem. *Eqs. (66)–(70) satisfy the following discrete energy dissipation law*

$$\mathcal{E}(\phi^{n+1}, \psi^{n+1}, r^{n+1}) \le \mathcal{E}(\phi^n, \psi^n, r^n), \tag{71}$$

where $\mathcal{E}(\phi^n, \psi^n, r^n) = \frac{\gamma_1}{2}\|\nabla\phi^n\|^2 + \frac{\gamma_2}{3}\|\nabla\psi^n\|^2 + r^n - C$.

Proof. Taking the L^2-inner product of Eq. (66) with $\Delta t\mu_\phi^{n+1}$, we get

$$(\phi^{n+1} - \phi^n) = -\Delta t M_\phi \|\nabla\mu_\phi^{n+1}\|^2. \tag{72}$$

Taking the L^2-inner product of Eq. (67) with $-(\phi^{n+1} - \phi^n)$, we have

$$\begin{aligned} -(\mu_\phi^{n+1}, \phi^{n+1} - \phi^n) &= -\gamma_1(\nabla\phi^{n+1}, \nabla\phi^{n+1} - \nabla\phi^n) \\ &\quad -(P^n r^n, \phi^{n+1} - \phi^n) \\ &= -\frac{\gamma_1}{2}(\|\nabla\phi^{n+1}\|^2 - \|\nabla\phi^n\|^2 \\ &\quad +\|\nabla\phi^{n+1} - \nabla\phi^n\|^2) \\ &\quad -(P^n r^n, \phi^{n+1} - \phi^n) - \frac{S_\phi}{\epsilon^2}\|\phi^{n+1} - \phi^n\|^2. \end{aligned} \tag{73}$$

Taking the L^2-inner product of Eq. (68) with $\Delta t\mu_\psi^{n+1}$, we have

$$(\psi^{n+1} - \psi^n, \mu_\psi^{n+1}) = -\Delta t M_\psi \|\nabla\mu_\psi^{n+1}\|^2. \tag{74}$$

Taking the L^2-inner product of Eq. (69) with $-(\psi^{n+1} - \psi^n)$, we obtain

$$\begin{aligned} -(\mu_\psi^{n+1}, \psi^{n+1} - \psi^n) &= -\gamma_2(\nabla\psi^{n+1}, \nabla\psi^{n+1} - \nabla\psi^n) \\ &\quad -(Q^n r^n, \psi^{n+1} - \psi^n) \\ &= -\frac{\gamma_2}{2}(\|\nabla\psi^{n+1}\|^2 - \|\nabla\psi^n\|^2 \\ &\quad +\|\nabla\psi^{n+1} - \nabla\psi^n\|^2) \\ &\quad -(Q^n r^n, \psi^{n+1} - \psi^n) \\ &\quad -\frac{S_\psi}{\eta^2}\|\psi^{n+1} - \psi^n\|^2. \end{aligned} \tag{75}$$

From Eq. (70), we have

$$r^{n+1} - r^n = (P^n r^n, \phi^{n+1} - \phi^n) + (Q^n r^n, \psi^{n+1} - \psi^n). \tag{76}$$

Combining Eqs. (66)–(70), we derive that

$$\begin{aligned} &\frac{\gamma_1}{2}(\|\nabla\phi^{n+1}\|^2 - \|\nabla\phi^n\|^2) + \frac{\gamma_2}{2}(\|\nabla\psi^{n+1}\|^2 - \|\nabla\psi^n\|^2) \\ &\quad +r^{n+1} - r^n \\ &= -\Delta t M_\phi \|\nabla\mu_\phi^{n+1}\|^2 - \Delta t M_\psi \|\nabla\mu_\psi^{n+1}\|^2 \\ &\quad -\frac{S_\phi}{\epsilon^2}\|\phi^{n+1} - \phi^n\|^2 - \frac{S_\psi}{\eta^2}\|\psi^{n+1} - \psi^n\|^2 \\ &\quad -\frac{\gamma_1}{2}\|\nabla\phi^{n+1} - \nabla\phi^n\|^2 - \frac{\gamma_2}{2}\|\nabla\psi^{n+1} - \nabla\psi^n\|^2 \le 0. \end{aligned} \tag{77}$$

The desired result is proved.

The proving process of unique solvability in Section 3.2 can be used for the first-order scheme (66)–(70) in a similar way, we will omit those similar steps for convenience.

References

[1] D. Myers, Wiley, Hoboken, 2006.
[2] H. Garcke, K.F. Lam, B. Stinner, Commun. Math. Sci. 12 (8) (2014) 1475–1522.
[3] H. Liu, Y. Zhang, J. Comput. Phys. 229 (2010) 9166–9187.
[4] S. Iglauer, Y. Wu, P. Shuler, Y. Tang III, W.A. Goddard, J. Pet. Sci. Eng. 71 (2010) 23–29.
[5] A.J. James, J. Lowengrub, J. Comput. Phys. 201 (2004) 685–722.
[6] J.-J. Xu, W. Shi, M.-C. Lai, J. Comput. Phys. 353 (15) (2018) 336–355.
[7] S. Shin, J. Chergui, D. Juric, L. Kahouadji, O.K. Matar, R.V. Craster, J. Comput. Phys. 359 (15) (2018) 409–435.
[8] W.-F. Hu, M.-C. Lai, C. Misbah, Comput. Fluids 168 (30) (2018) 201–215.
[9] R. Van der sman, M.B.J. Meinders, Comput. Phys. Comm. 199 (2016) 12–21.
[10] R. Guo, Y. Xu, SIAM J. Sci. Comput. (2021) http://dx.doi.org/10.1137/18M1235405.
[11] G. Soligo, A. Roccon, A. Soldati, J. Comput. Phys. 376 (2019) 1292–1311.
[12] M. Laradji, H. Guo, M. Grant, M.J. Zuckermann, J. Phys.: Condens. Matter 4 (1992) 6715–6728.
[13] S. Engblom, M.D. Quang, G. Amberg, A.-K. Tornberg, Commun. Comput. Phys. 14 (2013) 879–915.
[14] S. Gu, H. Zhang, Z. Zhang, J. Comput. Phys. 270 (2014) 416–431.
[15] X. Yang, J. Sci. Comput. (2021) http://dx.doi.org/10.1007/s10915-017-0508-6.
[16] X. Yang, L. Ju, Comput. Methods Appl. Mech. Engrg. 318 (2017) 1005–1029.
[17] G. Zhu, J. Kou, S. Sun, J. Yao, A. Li, Comput. Phys. Comm. 233 (2018) 67–77.
[18] G. Zhu, J. Kou, S. Sun, J. Yao, A. Li, J. Sci. Comput. (2021) http://dx.doi.org/10.1007/s10915-019-00934-1.
[19] M. Sun, X. Feng, K. Wang, Comput. Methods Appl. Mech. Engrg. 367 (2020) 113123.
[20] C. Xu, C. Chen, X. Yang, Numer. Algorithms (2021) http://dx.doi.org/10.1007/s11075-020-00915-8.
[21] J. Zhang, C. Chen, J. Wang, X. Yang, Comput. Phys. Comm. 251 (2020) 107122.
[22] Z. Liu, X. Li, 2019, arXiv preprint arXiv:2001.00812v1.
[23] Z. Xu, X. Yang, H. Zhang, Z. Xie, Comput. Phys. Comm. 238 (2019) 36–49.
[24] J. Zhang, X. Yang, Comput. Phys. Comm. 243 (2019) 51–67.
[25] Y. Gong, J. Zhao, Q. Wang, Comput. Phys. Comm. 249 (2020) 107033.
[26] Q. Li, L. Mei, Comput. Phys. Comm. (2021) http://dx.doi.org/10.1016/j.cpc.2020.107290.
[27] D. Hou, M. Azaiez, C. Xu, J. Comput. Phys. 395 (15) (2019) 307–332.
[28] W.J. Boettinger, J.A. Warren, C. Beckermann, A. Karma, Ann. Rev. Mater. Res. 32 (2002) 163–194.
[29] Y. Li, D. Jeong, H. Kim, C. Lee, J. Kim, Comput. Math. Appl. 77 (2019) 311–322.
[30] U. Trottenberg, A. Schuller, C.W. Oosterlee, Academic Press, 2000.
[31] X. Yang, Comput. Methods Appl. Mech. Engrg. 347 (2019) 316–339.
[32] J. Yang, J. Kim, Commun. Nonlinear Sci. Numer. Simul. 87 (2020) 105276.
[33] G. Zhu, H. Chen, J. Yao, S. Sun, Appl. Math. Model. 70 (2019) 82–108.
[34] Z. Guo, P. Lin, J. Lowengrub, S.M. Wise, Comput. Methods Appl. Mech. Engrg. 326 (2017) 144–174.